Journal of Marine Research, 62, 491–516, 2004

Observations and modeling of seasonal variability in the Straits of Georgia and Juan de Fuca

by Diane Masson[1] and Patrick F. Cummins[1]

ABSTRACT

The Strait of Georgia is a large semi-enclosed basin on the southern coast of British Columbia. Its main connection to the Pacific is to the south, through Juan de Fuca Strait. Abundant freshwater discharge, mainly from the Fraser River, forces an estuarine exchange with oceanic shelf water. The resulting circulation is modulated by tides and winds. Both the coastal wind stress and the flux of freshwater are subject to strong seasonal modulations, producing a marked seasonal cycle in the water properties and circulation of the region.

The seasonal variability of the Strait of Georgia and Juan de Fuca Strait is described using data from a series of recent cruises conducted over a five-year period, in addition to longer term historical data sets. To complement the observations, the data are compared with numerical simulations based on the Princeton Ocean Model (POM). Forced with tides, freshwater discharge and seasonal wind stress, the model is integrated over a few years until the system approaches statistical equilibrium. Results show good agreement with observations from Juan de Fuca Strait, as well as over the upper part of the water column within the Strait of Georgia. However, simulation of the seasonal cycle of the deeper waters of the Strait of Georgia is more problematic. The deep water properties apparently are determined by a delicate balance between dense intrusions from the sill area and local vertical mixing.

1. Introduction

The Straits of Georgia and Juan de Fuca are the two main bodies of water separating Vancouver Island and the mainland of the southern coast of British Columbia (Fig. 1). The Strait of Georgia is a semi-enclosed coastal basin that extends about 220 km along the coast with water depths of up to 420 m within its central deep basin. Its main connection with the open ocean is through Juan de Fuca Strait to the south, which is also the outlet for the Puget Sound Basin. Narrow channels between a series of small islands, as well as shallow sill areas, constrict the flow between the two straits, with most of the flow through the deeper western channel composed of Boundary Pass and Haro Strait. To the west, Juan de Fuca Strait opens up into a more regular channel-like basin of about 20 km width, reaching water depths of 250 m at its mouth. At its northern end, the Strait of Georgia is

1. Institute of Ocean Sciences, P. O. Box 6000, Sidney, British Columbia, Canada V8L 4B2. ***email: massond@dfo-mpo.gc.ca***

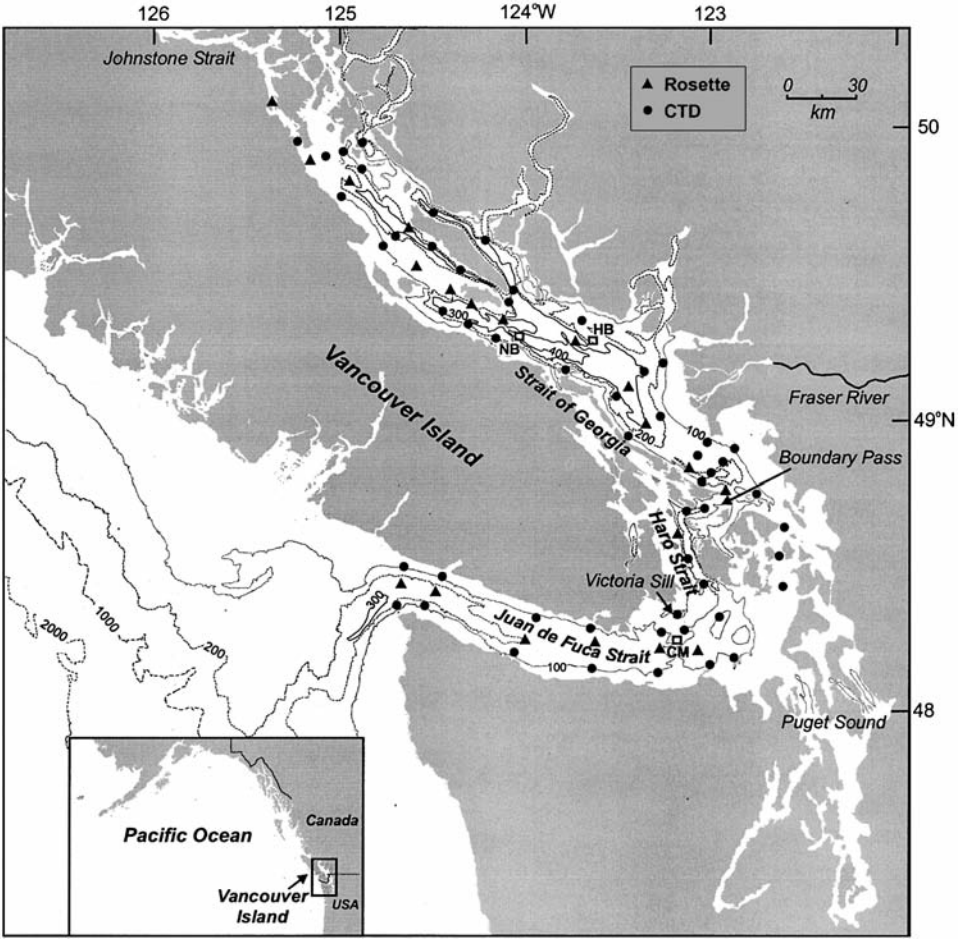

Figure 1. Coastline and depth contours (m) of the southern coast of British Columbia. **NB** indicates the Nanoose Bay station, **HB** the Halibut Bank meteorological buoy and **CM,** a near-bottom current meter. The small dots (CTD) and triangles (Rosette) indicate the stations of the seasonal survey program.

connected to the open ocean through constricted and shallow channels, with cross-sectional areas much smaller (7%) than those of the southern route (e.g., Waldichuk, 1957).

The three coastal basins form a large estuary in which a complex circulation is shaped by the basin morphology, a large and variable freshwater runoff, strong tidal currents and orographically steered coastal winds. Early descriptions of the physical oceanography of the Strait of Georgia and Juan de Fuca Strait were given by Waldichuk (1957) and Herlinveaux and Tully (1961), respectively. More recently, reviews of the region have been completed by Thomson (1981) and LeBlond (1983).

Rivers and small creeks discharge a significant amount of freshwater into these basins.

The most important source of freshwater is the Fraser River with its pronounced seasonal flow variations ranging from winter discharge rates as low as 300 $m^3\ s^{-1}$ to a maximum of over 10000 $m^3\ s^{-1}$ during spring freshet. Tides in the area are mixed, mainly semidiurnal, except near Victoria where there is a degenerate M_2 amphidrome and the diurnal component dominates (e.g., Foreman *et al.,* 1995). Strong tidal currents are found in constricted narrow and shallow passages and are associated with significant tide-induced mixing of the water column. This mixing is an important factor in regulating the exchange between the coastal basins and it produces a marked fortnightly modulation of the estuarine circulation (e.g. Griffin and LeBlond, 1990; LeBlond *et al.,* 1994; Masson and Cummins, 2000).

Seasonal wind variability is mostly determined by two main atmospheric pressure systems (e.g. Thomson, 1981). In winter, the Aleutian Low predominates, producing strong south-to-southeasterly winds. This gives way during summer months to the North Pacific High with its weaker northwesterly winds. Associated with the seasonal change in dominant wind direction is a transition from downwelling (winter) to upwelling (summer) conditions over the continental shelf (e.g. Freeland *et al.,* 1984). As a consequence, the deep estuarine return flow is colder and saltier (denser) during summer. These changes in both freshwater runoff and atmospheric forcing modulate significantly the estuarine circulation of the coastal basin at the seasonal time scale.

In this paper, we combine new observations from a series of recent cruises with historical data to describe the mean properties and the seasonal variability of the salinity field and the circulation of the Straits of Georgia and Juan de Fuca. In 1999, a field program was established to sample the estuary a few times each year. Each survey consisted of a set of 73 stations, extending from the mouth of Juan de Fuca Strait up to the northern end of the Strait of Georgia (Fig. 1). CTD profiles were recorded at each station and water samples collected at a subset of stations lying along the main axis of the estuary. A total of 19 surveys were conducted over the five-year period, 1999–2003 (Fig. 2). An attempt was made to time the surveys with the seasonal freshwater cycle. Sampling is preferentially done during periods of (1) low winter discharge, (2) early freshet (April), (3) peak freshet (early summer), and (4) end of freshet period (early fall).

The observations are presented in the context of a comparison with simulations obtained with a three-dimensional, baroclinic numerical model. In particular, results from the Princeton Ocean Model (POM) are compared extensively with the observed seasonal variability. The model is used to estimate volume transports, which are difficult to infer from the data. Dynamical processes, such as the influence of tidally-induced mixing on the overall density structure, are examined in sensitivity experiments. Different versions of the model have been used to investigate some features of the local circulation such as the fortnightly modulation of the estuarine circulation within Juan de Fuca Strait (Masson and Cummins, 2000), and the development of the Vancouver Island Coastal Current (Masson and Cummins, 1999).

Previous modeling studies of the region include the simplified box model developed by

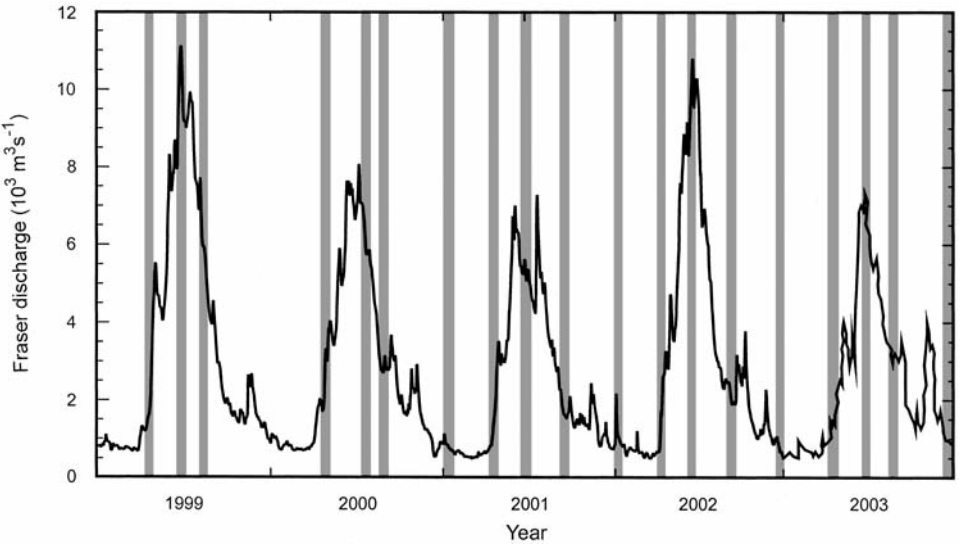

Figure 2. Fraser River discharge (daily mean) measured at Hope, BC. The shaded bars indicate the timing of the 19 oceanographic surveys conducted between 1999 and 2003.

Li *et al.* (1999) to examine the seasonal and interannual variability of the local circulation. They found that the salinity distribution is mostly determined by the river runoff and vertical mixing, and that the system adjusts to a change in forcing within a year, in close agreement with previous estimates (e.g. England *et al.,* 1996). Marinone and Fyfe (1992) developed a 2-D circulation model of the area forced by tides only. This was extended subsequently by Marinone *et al.* (1996) to a 3-D grid forced by tides, wind and runoff. Their study focused on the low-frequency residual currents in the central part of the Strait of Georgia.

In this paper, multi-year simulations are presented. These follow the standard perpetual year methodology which consists in repeating a fixed climatological seasonal forcing year after year. A similar approach has been applied to other coastal ocean regions such as the Mediterranean (Beckers *et al.,* 2002) and the Adriatic Sea (Zavatarelli *et al.,* 2002). To our knowledge, this work presents the first 3-D numerical simulations of the local dynamics of the Straits of Georgia and Juan de Fuca at seasonal time scales.

2. The model

This study makes use of the POM, a three-dimensional, sigma co-ordinate, numerical ocean model (Blumberg and Mellor, 1987). It solves second-order accurate, finite difference analogs of the primitive equations. A level 2.5 turbulence closure scheme provides the vertical mixing coefficients (Mellor and Yamada, 1982). The model is widely used and has proven its utility in numerous coastal ocean situations (e.g. Young *et al.,* 2003). It is

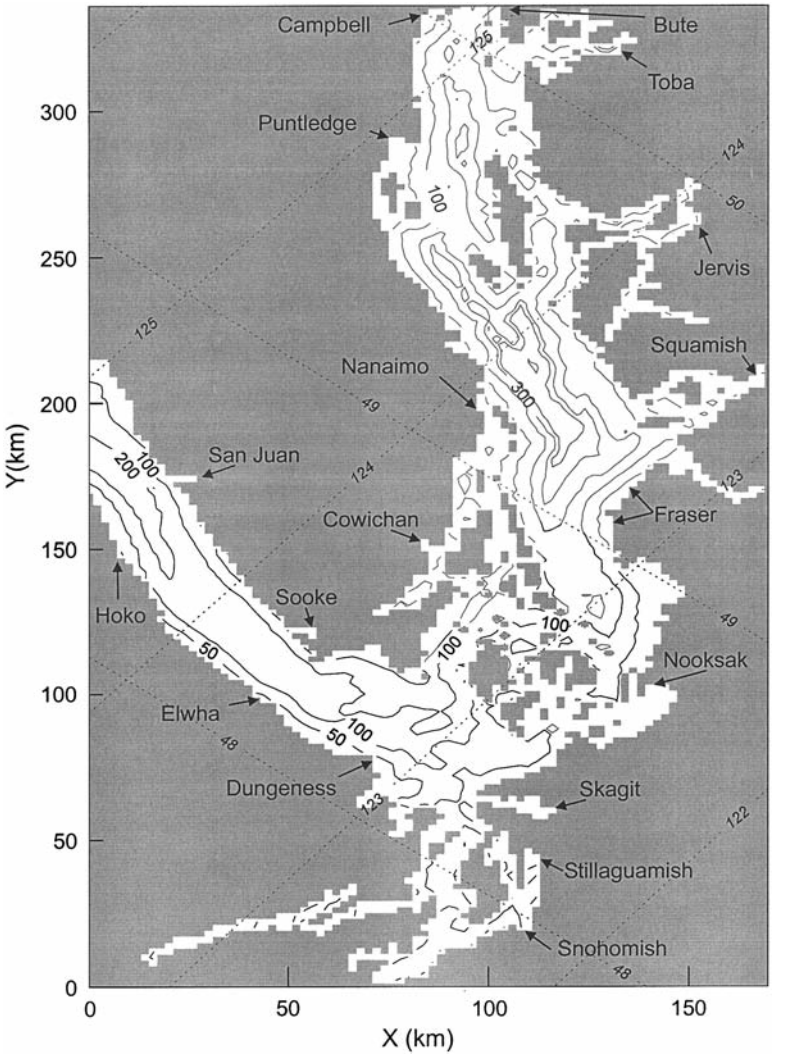

Figure 3. Model grid including the locations of rivers.

applied here with a Cartesian grid covering an area of (172 × 338) km, with a uniform horizontal resolution of 2 km. The model grid includes the Straits of Georgia and Juan de Fuca, along with northern Puget Sound (Fig. 3). A clockwise rotation of 40° from True North has been applied to align approximately the main axis of the Strait of Georgia with the y-coordinate of the model grid. There are 31 sigma levels in the vertical, with enhanced resolution near the surface and bottom. The horizontal viscosity and diffusivity are parameterized by the standard Smagorinsky formulation. Given the relatively fine grid resolution, a small value of the nondimensional Smagorinsky coefficient, HORCON =

0.03, is used here to minimize the classical problem of spurious diapycnal diffusion that occurs where isopycnal surfaces intersect the sigma levels of the model. Sensitivity of the model results to the HORCON parameter is discussed below, in Section 3c. The model domain includes two open boundaries, at the mouth of Juan de Fuca Strait and at the northern end of the Strait of Georgia.

Initially, the model ocean is quiescent and homogeneous with uniform salinity (30 psu) and temperature (8°C). The integrations are performed in a prognostic mode, allowing the density field to adjust freely to the forcing. As in most estuaries, local variations in water density are largely determined by the salinity. Therefore, for simplicity, the temperature equation is not solved and the water temperature remains at $T = 8°C$ throughout the integration.

The Fraser River has important seasonal variations dominated by a large peak freshet discharge in June associated with snowmelt. On the other hand, rivers discharging into Juan de Fuca Strait and Puget Sound have increased runoff in winter due to local rainfall and during the spring freshet. Based on estimates made by LeBlond *et al.,* 1983, Figure 4a gives the climatological seasonal discharge for the three basins: the Straits of Georgia and Juan de Fuca and Puget Sound. A total of 19 rivers have been included in the model (see Fig. 3 for river locations). The Fraser River alone accounts for about 50% of the total river runoff into the estuary. For each of the three basins, the total discharge into the basin has been distributed among the local rivers in proportion to their known mean annual discharge. Also, each river, depending on its location, follows one of the three time-dependent seasonal cycles indicated in Figure 4a.

The model is driven at the two open boundaries with the four leading tidal constituents, K_1, O_1, M_2, and S_2 through a forced gravity wave radiation condition on the normal component of the depth-integrated velocity (Flather, 1987). In the modeled area, these four tidal constituents generally account for about 70% of the tidal stream velocity (Crean *et al.,* 1988). The resulting tides are subject to a spring-neap cycle which arises through an interference of both the two semidiurnal and of the two diurnal constituents. Tides are included in the present context of seasonal variability because of the importance of the tidally induced mixing in controlling the estuarine circulation.

At the mouth of Juan de Fuca Strait, as well as at the northern end of the Strait of Georgia, a radiation condition is used to specify the baroclinic component of normal velocity. An upstream advection scheme determines the salinity at outflow points. Salinity is specified on the time-dependent inflow points of the open boundaries. At the mouth of Juan de Fuca Strait, the seasonal cycle of the inflow salinity is important in setting periods of deep water renewal (Masson, 2002). During summer, upwelling on the shelf provides colder and saltier (denser) water at depth. On the other hand, in winter, due to predominantly downwelling winds, warmer and relatively less saline (less dense) water enters the estuary at depth.

To specify the salinity at inflow points along the open western boundary, mean monthly salinity profiles were calculated from a set of 530 hydrographic casts collected near the

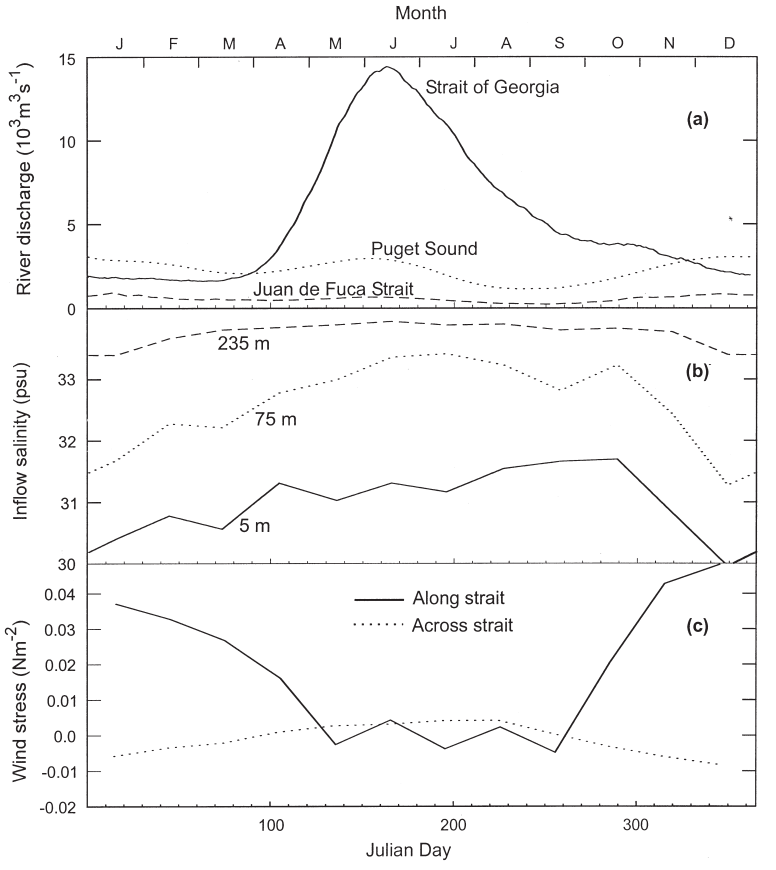

Figure 4. Model seasonal forcing: (a) river discharge for the Strait of Georgia (full line), Puget Sound (dotted line) and Juan de Fuca Strait (dashed line) basin; (b) mean monthly salinity of the inflow at the mouth of Juan de Fuca Strait measured at 5 m (full line), 75 m (dotted line), and 235 m (dashed line) depth; and (c) mean monthly wind stress measured at Halibut Bank, for the along-strait (full line) and across-strait (dotted line) direction.

mouth of Juan de Fuca Strait between 1938 and 2001. The historical hydrographic casts used in this study have been extracted from the data archive of the Institute of Ocean Sciences. The water column was divided into 10 m intervals for which mean monthly salinity values were computed. In Figure 4b, the resulting monthly salinity values are given for three representative depths: at the surface (5 m), near the inflow/outflow transition depth (75 m), and close to the bottom (235 m). Below the surface, salinity values reach a maximum during the summer upwelling season. At the surface, salinity values peak later, in early fall, when the intensity of local rainfall is still relatively low and the upwelling on the shelf is weaker. For the model integration, linear interpolation between adjacent months and depth intervals was used to compute the daily salinity values of the inflow for each model grid cell along the open western boundary.

Less information is available on the properties of the water entering the domain from the northern end of the basin. Thomson (1976) discussed the general structure of the estuarine circulation in Johnstone Strait (see Fig. 1) from a series of measurements. He found that the annual range of salinity within the western section of the strait is small, varying between 31 and 32 psu near the bottom. A similar range was also observed in the vicinity of the model northern boundary during the more recent seasonal surveys. In keeping with these observations, the inflow salinity is held constant at a value of 31.5 psu along the northern boundary of the model.

At the surface, a spatially uniform wind stress is applied. A seasonal climatology was obtained by computing monthly means of the wind stress measured at Halibut Bank (Fig. 1) for the 10 year period of 1992 to 2001 (Fig. 4c). In reality, the momentum flux over the study area is influenced by the complex local orography. However, it is believed that, owing to its central location and because we are interested in relatively long time scales, the wind measured at the meteorological buoy should be representative of the general wind forcing over the Strait of Georgia. The wind stress time series of Figure 4c reflects the large-scale orographic control of the wind field with a dominant along-strait wind component. It also shows the shift from strong southeast winds during winter to weaker northwest winds in summer.

3. Comparison with observations

The numerical model described above was used in a series of multi-year numerical experiments in which the climatological seasonal forcing is repeated from year to year. We first compare the observations with results of the mean and seasonally varying circulation from a basic case. This experiment, which was integrated for a period of three years, includes forcing with tides, seasonally varying freshwater runoff, western boundary inflow salinity and wind stress, as illustrated in Figure 4. This is followed by a discussion of results from a series of sensitivity experiments where the effect of varying several forcing functions and parameters is investigated.

a. Mean circulation

Time series of the salinity, averaged laterally over the model domain, were computed for the whole water column, as well as for the five sigma levels nearest the surface and adjacent to the bottom (Fig. 5). The change in surface freshwater content of the estuary is controlled by the cycle of the freshwater discharge, with the minimum average salinity occurring shortly after the freshet in June. At depth, the signal is a combination of the freshening at the surface from river discharge and the change in salinity of the incoming shelf water. This leads to two annual salinity minima: one in early summer due to the freshet and a second small one in winter during the downwelling season. A similar seasonal variability has been observed by Waldichuck (1957) within the Strait of Georgia and is present in the recent survey data (see Fig. 13). At longer time scales, the system appears to

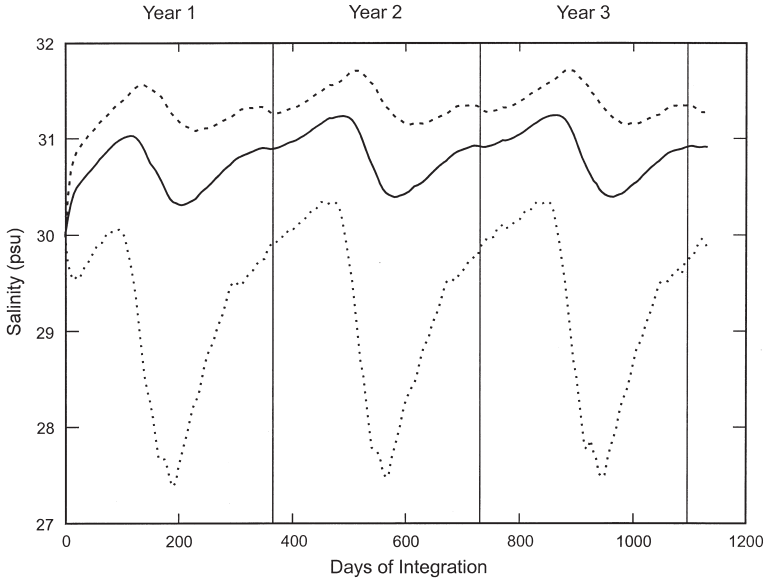

Figure 5. Average salinity for the reference experiment for the whole basin (full line), the top 5 (dotted line) and the bottom 5 (dashed line) sigma layers.

adjust fully to the forcing within the first year, with a seasonal cycle virtually unchanged from the second year to the third one. This is consistent with Li *et al.* (1999) who found that conditions within their box model adjusted to changes in river runoff within one year. Accordingly, in the following analysis, results from the second or, when available, from the third year of the numerical experiments are used for comparisons with the observations.

The first assessment of the model's ability to simulate the local dynamics concerns an evaluation of the simulated tidal elevations. Results for the four constituents, K_1 O_1 M_2 and S_2, are in general agreement with the results of Foreman *et al.* (1995) who successfully simulated tides in eastern Juan de Fuca Strait and the southern Strait of Georgia with a three-dimensional, barotropic, finite element model. In particular, the model reproduces the most notable local features such as the degenerate M_2 amphidrome near Victoria, the quasi-stationary M_2 phase in the Strait of Georgia, and the monotonic increase of K_1 amplitudes from the entrance of Juan de Fuca Strait to the northern end of the Strait of Georgia. Table 1 gives the average relative and absolute rms differences between observed

Table 1. Average absolute and relative differences between observations at 44 tide gauge sites and corresponding model results for each tidal constituent used to force the model.

Tidal components	K_1	M_2	O_1	S_2
Absolute error, D (cm)	1.7	5.5	1.8	2.5
Relative error, D/A_o (%)	2.2	3.5	3.9	13.7

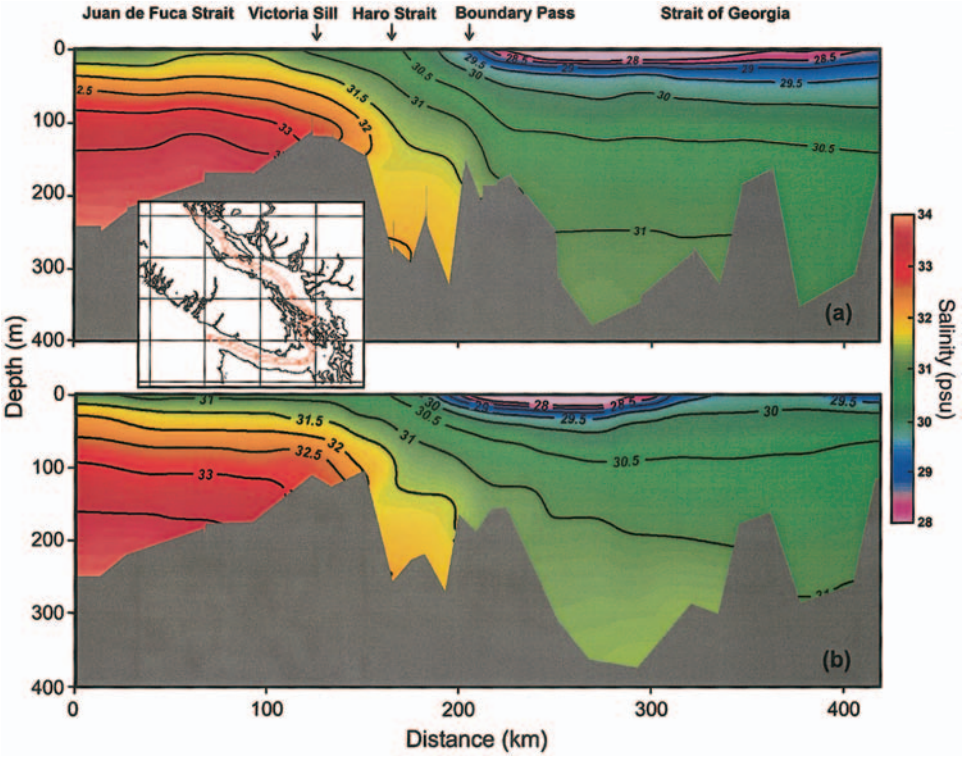

Figure 6. Along-strait section of annual mean salinity from observations (a) and the reference experiment (b).

and calculated sea level amplitudes and phases at 44 tide gauge sites distributed over the region. At each site, the rms difference between the model and observations, D, was computed according to

$$D = \left[\frac{1}{2} (A_m^2 + A_o^2) - A_m A_o \cos(\phi_m - \phi_o) \right]^{1/2}, \quad (1)$$

where A_m and A_o are the sea level amplitude of the model and observations, respectively, while ϕ_m and ϕ_o are the respective phases. The errors indicated in Table 1 are comparable with those of previous studies and it indicates that the tides are represented with a sufficient degree of accuracy to satisfy the objectives of this study.

We now consider the mean salinity field. Model results are compared with an observed climatology obtained from the seasonal sampling program. Figure 6 gives contours of mean salinity along the main axis (thalweg) of the estuary from observations (a) and the base numerical experiment (b). The average of the numerical solution is based on results from the third year of integration and, in order to correspond to the observational mean, the average was obtained using salinity values for the month of January and for the April to

September period. The comparison demonstrates that the modeled ocean displays a realistic salinity (and density) structure. It includes the main features of the observed mean state: the freshwater surface plume in the Strait of Georgia, the dense near-bottom inflow into Juan de Fuca Strait, reduced stratification in Haro Strait, the surface front at Boundary Pass, and the deep front over Victoria Sill. Also, the model maintains a lateral salinity gradient along the thalweg that is close in magnitude to the observed one for both the surface outflow and for the deeper layer. The comparison also reveals some discrepancies. In particular, the deep basin of the Strait of Georgia is observed to be slightly fresher (by about 0.2 psu) than in the model. Similarly, the surface layer observed over the northern Strait of Georgia is somewhat fresher than in the simulation. But, overall, the numerical model appears to capture the salient aspects of the hydrography of the region under the prescribed seasonal forcing.

The across-channel structure of the estuarine flow is now examined by comparing the observed and modeled salinity during July along a section spanning Juan de Fuca Strait. In Figure 7a, average salinity values have been computed from about 150 profiles along the transect, collected in the month of July over a 15-year period (1987–2001). Figure 7b gives the average salinity for July from the third year of the model simulation. At this time of year, the freshwater discharge is near maximum and the estuarine flow at maximum strength. The summer density structure follows the classical two-layer estuarine flow with the top fresh layer flowing over the deep oceanic return flow. The cross-channel slope of the isohalines is consistent with the vertical shear associated with a geostrophically balanced inflow at depth and outflow at the surface under the thermal wind relation.

The model indicates a significant along-strait variation in the cross-strait structure of the flow. This is associated with cross-strait flows and meandering of the surface outflow. Both the vertical salinity range (30.4 to 33.8 psu) and the slope of the isohalines are well represented by the model. However, the CTD profiles reveal a more sharply defined halocline between the top inflow and bottom return flow. In the case of the numerical solution, the halocline is more diffuse, pointing to possible excess vertical mixing produced by the mixing parameterization.

In the Strait of Georgia, energetic low-frequency current fluctuations are known to exist (e.g. LeBlond, 1983). Stacey *et al.* (1987) show that mean residual currents observed from June 1984 until January 1985 form a cyclonic gyre in the central part of the Strait. The gyre was present at 100, 200 and 290 m depth across their measurement array which had a lateral extent of 10 to 15 km (see Fig. 8). The cyclonic circulation had flow speeds of about 10 cm s^{-1}, and the gyre tended to follow the topographic contours near the bottom. This is one of the few well documented features of the subsurface circulation in the Strait of Georgia. Attempts have been made to reproduce the observed mean residual currents with a local depth-integrated model forced by a number of tidal harmonics (Marinone and Fyfe, 1992). The mean residual velocities of their model formed a cyclonic eddy but underestimated its strength by about an order of magnitude. Subsequently, Marinone *et al.* (1996) developed a 3-D baroclinic model forced by winds, tides and runoff which also shows

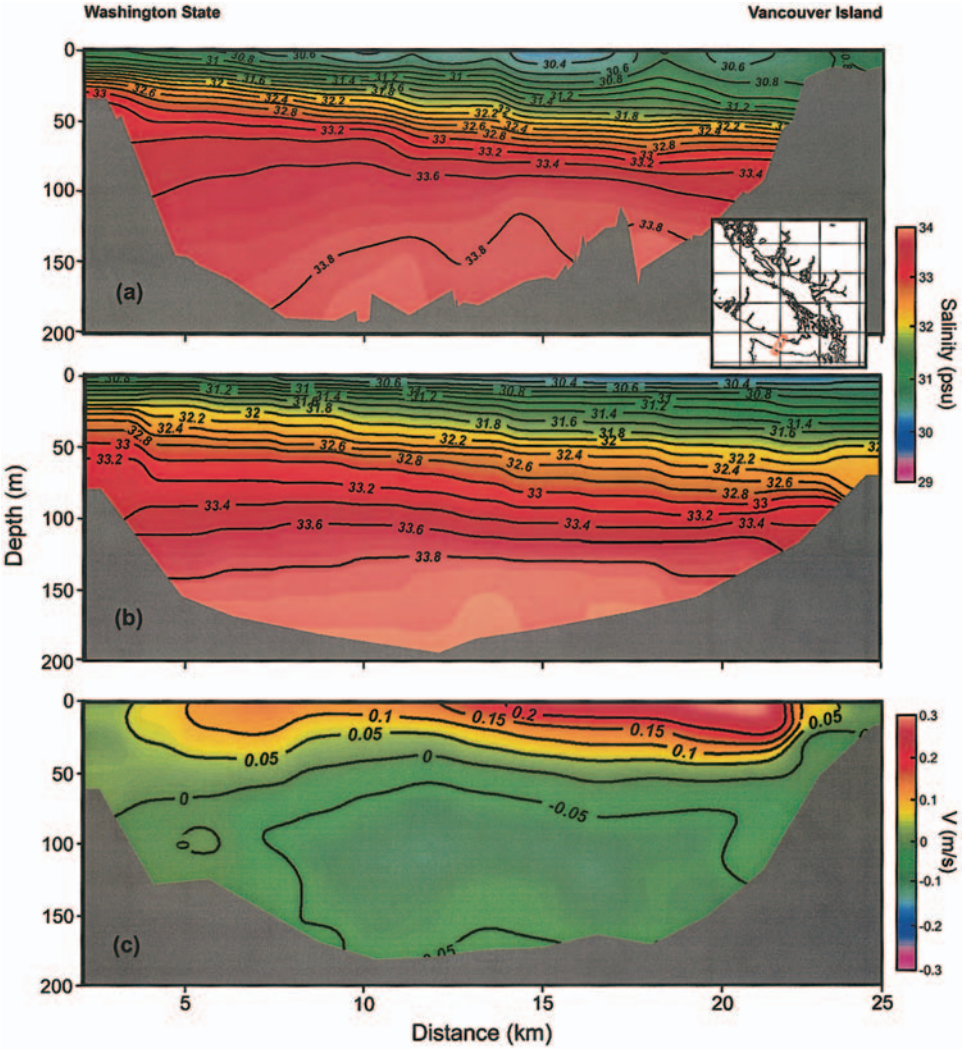

Figure 7. Mean salinity (a and b) and along-strait velocity (c) for the month of July, along a section spanning Juan de Fuca Strait. The observations are shown in (a) while results from the reference experiment are given in (b) and (c). Positive velocities indicate flow out of the estuary.

mean residual velocities considerably smaller than observed and with the direction of the flow only agreeing in some locations. Holloway (1993) suggested that the absence of statistical-dynamical tendencies could be partly responsible for the weak response in their model.

Figure 8 gives mean velocity vectors at a depth of 100 m averaged over the third year of the basic experiment. The model residual currents form a pair of gyres within the central

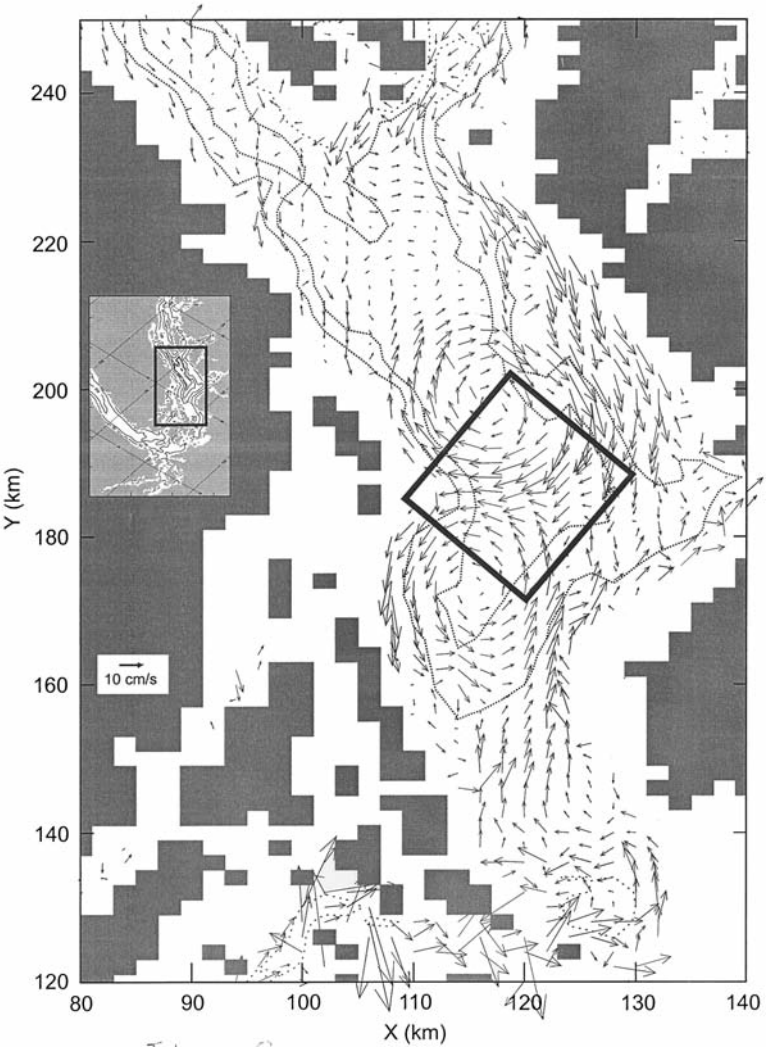

Figure 8. Mean velocity vectors at 100 m depth for the third year of the basic experiment. The square indicates the position of the observational array of Stacey *et al.* (1987). The insert shows the section of the grid used.

Strait of Georgia, cyclonic in the south and anticyclonic in the north. They are baroclinic gyres with a horizontal scale comparable to the local internal deformation radius which varies from 8 to 7 km from summer to winter. The modelled gyres persist throughout the year, with increased strength during the summer high discharge period. Although the position of the southern cyclonic gyre in Figure 8 is about 10 km south of the one observed by Stacey *et al.* (1987), it is of comparable dimensions and intensity, with scale velocity of

about 10 cm s^{-1}. Results of the various sensitivity runs described below indicate that the double gyre circulation is a robust feature of the modeled circulation. The eddies are present in all the numerical experiments, including the cases without wind or tidal forcing. This suggests that the residual currents observed by Stacey *et al.* (1987) are driven primarily by buoyancy forcing associated with the freshwater runoff, while the effects of the tides and the wind stress are of secondary influence.

b. Seasonal variability

In the preceding section, various features of the observed mean state were compared with model results. We now explore the ability of the model to reproduce the seasonal variability of the system under time-dependent forcing. In Figure 9, the evolution of the vertical salinity profile through the year is compared with model results for an area located midway along Juan de Fuca Strait. The model results are an area average computed from the third year of the basic case, while the observed field is a composite of about 1500 CTD casts measured between 1977 and 2002. Figure 9 indicates that the two-layer estuarine nature of the flow as well as the overall seasonal variation in the local stratification is captured by the model. At the surface, summer and winter salinity minima are associated with freshet and local winter rainfall, respectively. On the other hand, the salinity of the deep return flow is determined by the succession of summer upwelling and winter downwelling periods, resulting in a deep salinity maximum in July and a minimum in December. Although the model captures most of features of the seasonal cycle, there are also marked differences. For example, the model surface layer is not sufficiently fresh in winter, which may indicate an underestimation of the winter freshwater flux, probably associated with rainfall and local discharge into the strait. Also, the layer of dense upwelled water present in summer near the bottom is not quite as thick as in the observations.

Within Haro Strait, the seasonal variability in vertical stratification bears similarities to that observed in Juan de Fuca Strait. In both the observations and the model results, salinity is slightly lower at the surface during summer freshet and increases near the bottom during the summer upwelling season (Fig. 10). Again, the seasonal cycle is formed through an area average of a large number of CTD casts (830) measured between 1977 and 2002 (Fig. 10a). The numerical results are drawn from the third year of the basic numerical experiment (Fig. 10b). The water column in the strait tends to be more strongly stratified from about mid-April to mid-October (e.g. Li *et al.,* 1999). However, because Haro Strait is an area of intense tidal mixing, observed seasonal variations are strongly modulated by the tides. Measured profiles vary depending on the stage of the tide (e.g. Webster, 1977), leading to the pronounced intra-seasonal variability in the measured salinity contours of Figure 10a. Model results of Figure 10b are also affected by the local tidal mixing, evidenced by the fortnightly modulations in the salinity contours. In contrast with the observations, the numerical output displays a regular 15-day signal because the sampling was done over a single year as opposed to the multi-year period over which the data were collected. The fortnightly modulations also occur downstream in Juan de Fuca Strait

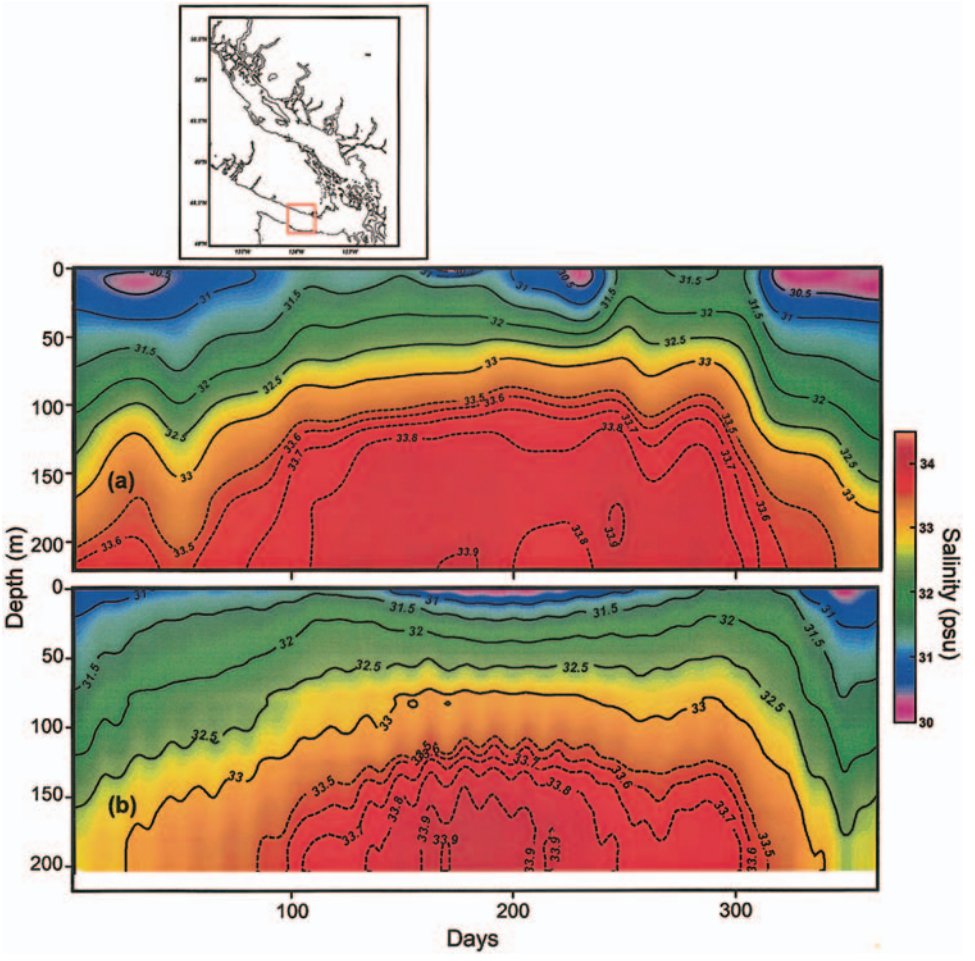

Figure 9. Observed (a) and modeled (b) seasonal cycle of vertical salinity profile averaged over a box situated midway along Juan de Fuca Strait.

(Fig. 9b), but with an amplitude decreasing with distance from the intense mixing area (as in Masson and Cummins, 2000).

Since the system is subject to a large reduction of freshwater discharge from summer freshet to winter (Fig. 4a), the strength of the estuarine circulation may also be expected to vary significantly through the year. Figure 11a displays a record of the deep return current as measured by a current meter situated near the bottom on Victoria Sill, in the eastern section of Juan de Fuca Strait (location CM on Fig. 1). The current meter was an Aanderra RCM4 deployed 10 m off the bottom in water of 90 m depth. The along-strait velocity in Figure 11a is based on daily averages of de-tided currents measured over a period of about 17 months starting in April, 1989 (dotted line). The tidal signal was removed using

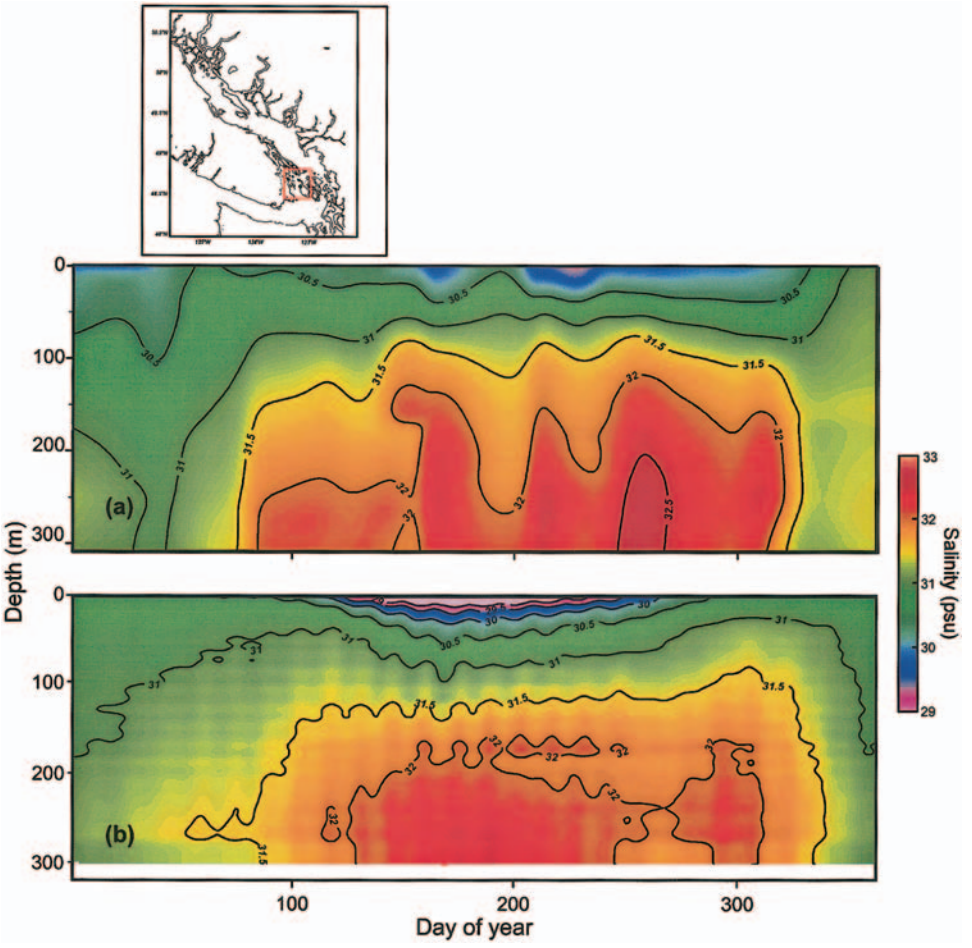

Figure 10. Observed (a) and modeled (b) seasonal cycle of vertical salinity profile averaged over the Haro Strait area.

harmonic analysis, but retaining longer sub-diurnal components. A low-passed version of the residual is also included in Figure 11. Particularly evident is the fortnightly variability of the deep current induced by the tidally modulated mixing over the shallow sills (e.g. Webster, 1977; Masson and Cummins, 2000). The velocities are also modulated on an annual cycle by the change in buoyancy forcing, with values varying from a maximum of 20 cm s^{-1} in summer down to about 10 cm s^{-1} during winter, as evidenced by the low-passed time series (full line).

Figure 11b gives daily average transport, computed from de-tided hourly model velocities obtained in the second and third year of the basic experiment. Transport values have been estimated across a section located in central Juan de Fuca Strait and near the

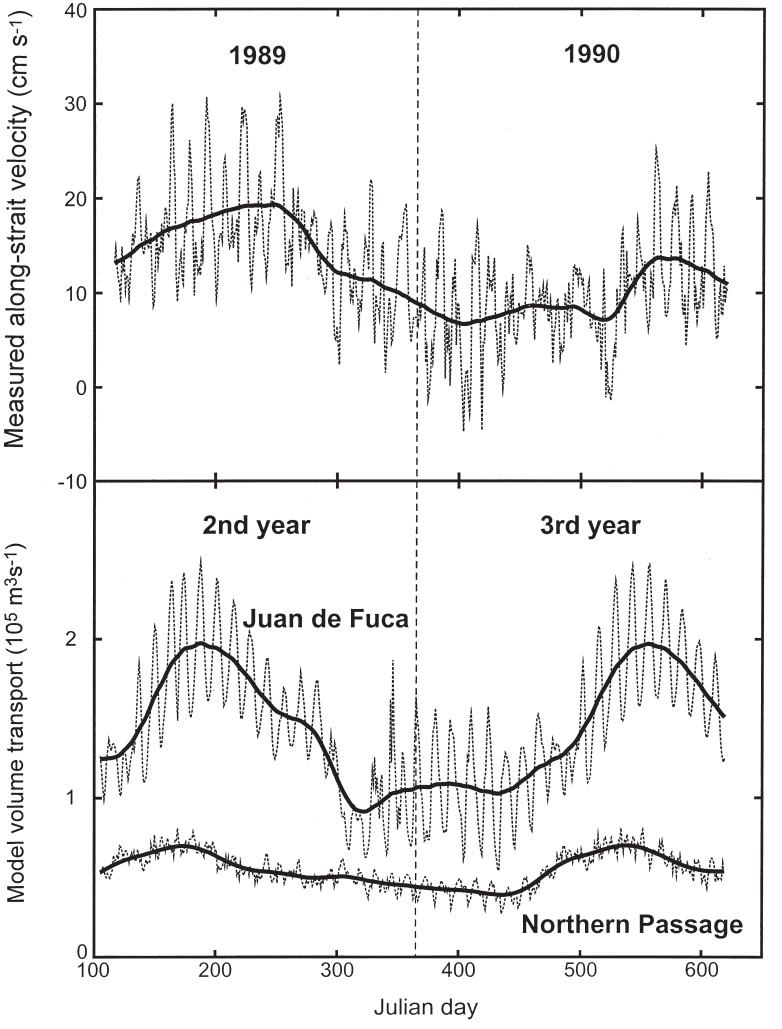

Figure 11. Time series of de-tided daily averages of the velocity along the thalweg (60° True) near the bottom at CM (a), a current meter situated on Victoria Sill (see Fig. 1). The current meter was an Aanderaa RCM4 deployed 10 m off the bottom in 90 m depth. The thick line is the low-pass filtered signal. In (b), mean daily transport computed from the model results of the 2nd and 3rd year of the basic run is indicated by the dotted line for both a section across Juan de Fuca Strait and the northern end of the model domain. Thick lines indicate the low-pass filtered signal.

open boundary in the northern end of the estuary. The full line gives the low-pass filtered signal of the transport. Firstly, it appears that the model results are consistent with previous estimates of the transport in both Juan de Fuca Strait (0.9 to 1.6 $\times$ 10^5 m^3 s^{-1}) and Johnstone Strait (0.15 to 0.5 $\times$ 10^5 m^3 s^{-1}) (e.g. LeBlond, 1983). Secondly, the variability of the model transport within Juan de Fuca Strait is in qualitative agreement with the

observations of Figure 11a, with regard to both the fortnightly modulation and the annual signal. Also evident in Figure 11b, is that the exchange is significantly larger in the southern access to the estuary. As mentioned above, this is to be expected given the much smaller cross-section of the northern channels.

The above results can be compared with estimates provided by the simple Knudsen relations. Assuming steady state, the conservation of mass and salt gives, respectively,

$$Q_2 + R = Q_1 \text{ and } Q_1 S_1 = Q_2 S_2, \tag{2}$$

where R is the river discharge rate, Q, the volume transport leaving (Q_1) and entering (Q_2) the estuary. S_1 and S_2 are the (uniform) salinities of the outflowing and inflowing water, respectively. From (2), the ratio of the deep inflow volume transport from summer to winter is given by

$$\frac{Q_{2_{\text{summer}}}}{Q_{2_{\text{winter}}}} = \frac{R_{\text{summer}}}{R_{\text{winter}}} \frac{\left(\frac{S_2}{S_1} - 1\right)_{\text{winter}}}{\left(\frac{S_2}{S_1} - 1\right)_{\text{summer}}}. \tag{3}$$

Using the freshwater discharge rates of Figure 4a and defining summer as the period June to August and winter as January to March, we obtain a ratio of summer to winter river discharge of 2.6. Considering the part of the estuary upstream from the area where the instrument CM was deployed (and neglecting the exchange at the northern boundary), the required salinity values can be estimated from the salinity profiles of Figure 9a, with $(S_2/S_1)_{\text{summer}} = (33.8/32)$ and $(S_2/S_1)_{\text{winter}} = (33/31.5)$. Eq. 3 then implies a reduction of the volume transport in winter by a factor of about 2.2 relative to that of the summer. This estimate is consistent with the seasonal change of speeds presented in Figure 11 where both the observations and the model simulation indicate an approximate doubling of the strength of the deep return flow in summer.

Moving upstream within the estuary, we now examine seasonal variability within the Strait of Georgia. Figure 12a gives the annual cycle of salinity at the Nanoose Bay station located in the deep central basin of the Strait of Georgia (NB in Fig. 1). The observed seasonal changes in the vertical salinity distribution were obtained from 225 profiles taken at the Nanoose Bay station, over a five year period starting in January 1999. This station is regularly sampled a few times a week throughout the year. At the surface, salinity reaches its minimum value a few weeks after the Fraser River freshet. There is also a secondary surface salinity minimum in December due to abundant local winter rainfall. On the other hand, the seasonal range of salinity of the deep basin is much smaller. Values remain slightly above 31 psu throughout the year; maximum values of about 31.4 psu are attained during the fall deep water renewal season (e.g. Masson, 2002). Salinity values at sill depth, which is around 100 m (the minimum depth at Boundary Pass) remain quite close to 30.5 psu throughout the year, with a slight minimum in spring.

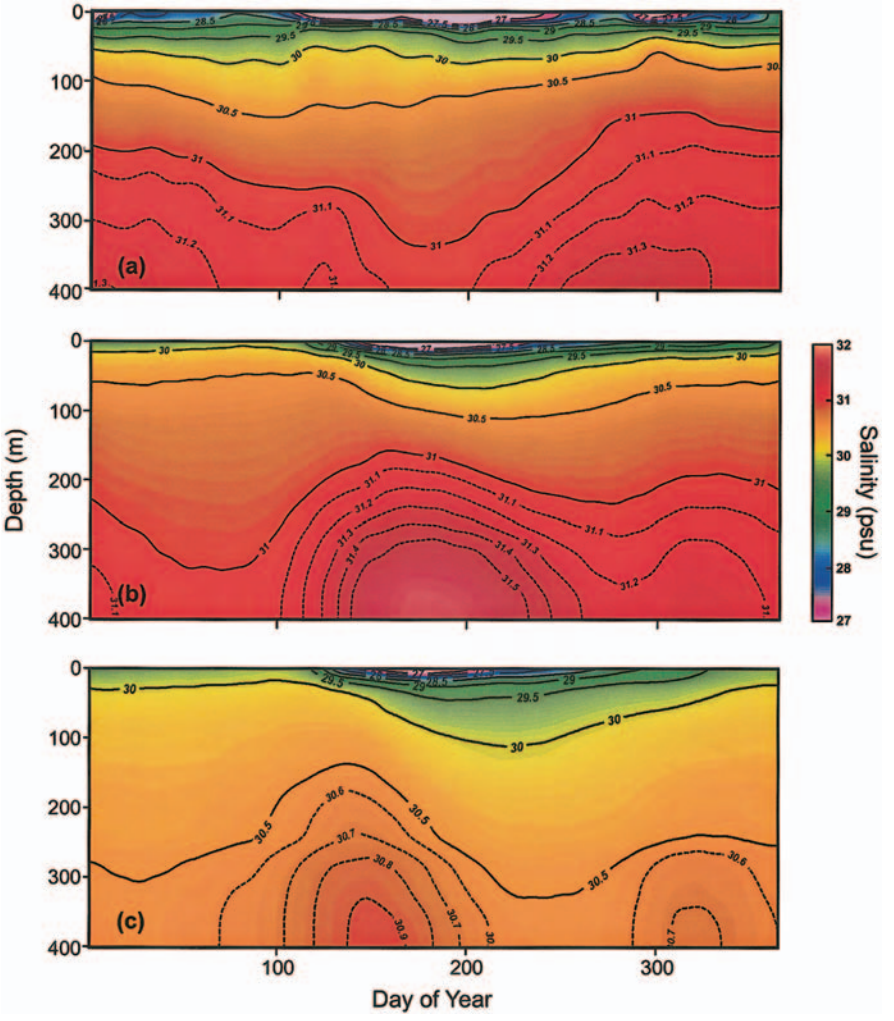

Figure 12. Observed (a) and modeled (b and c) seasonal cycle of vertical salinity profile at the Nanoose Bay station in the Strait of Georgia (identified as **NB** in Fig. 1). In (b), HORCON is set to 0.03 (reference experiment), and in (c) it is doubled to a value of 0.06.

The changes in salinity profiles in the vicinity of the station obtained from the third year of the basic experiment are given in Figure 12b. Overall, the model salinity values and stratification are close to the observations. The intensification of the surface plume produced by the freshet river discharge is well represented. However, the phase of the seasonal changes in the deep layer defers markedly from the observations. The model indicates that the near-bottom salinity reaches a maximum in early summer associated with an intensified deep water renewal episode. During the same period, observations show a

salinity minimum occurring between the spring and the stronger fall deep water renewal seasons. Changes in the observed properties of the deep water are the result of a delicate balance between the inflow of dense water advected landward over the sill and the level of mixing with the fresher upper water mass. As will be discussed below, this aspect of the local dynamics is sensitive to the level of diapycnal mixing in the model. In addition, some aspects of the deep water renewal process may also depend on seasonal variations in the temperature of the different water masses involved. However, despite the difficulty in reproducing the seasonal cycle, the mean salinity of the deep basin obtained in the basic experiment is quite close to the observations, as indicated in Figure 6.

c. Sensitivity experiments

In the preceding discussion, the observations were compared with results of a reference experiment for which the seasonal forcing and the various model parameters were fixed. We now examine the sensitivity of the numerical results to changes to some of these model characteristics. In the first experiment, a change in freshwater forcing is imposed, with all river discharges increased by 50% over the reference case. As expected, the stronger buoyancy forcing increases the freshwater content within the estuary. Figure 13 gives the volume of freshwater contained in the coastal basin for the basic experiment as well as for the case of increased river discharge. Also included in the figure are estimates of the freshwater volume computed from CTD profiles taken during the 19 hydrographic surveys, over the period 1999–2003. For both field data and model results, the freshwater content, V_{fw}, is a volume integral over the entire study region:

$$V_{fw} = \int\int\int_{V} \frac{(S_{ref} - S)}{S_{ref}}\, dV. \tag{4}$$

The value of the reference oceanic salinity, S_{ref}, is set to 33.8 psu, the maximum salinity of the inflow from the shelf. The resulting annual cycle for V_{fw} shows two peaks for both data and model results. There is a winter maximum associated with reduced salinity influx from the shelf during the downwelling season, and a summer maximum caused by the large freshet river discharge. The data show pronounced year-to-year variability, which is linked to inter-annual changes in river discharge (see small bar plot in Fig. 13). The model results of the basic case, where the river discharge was set to the long term mean, do capture the two annual maxima but with an overall level close to that measured during 2001, a year of relatively low river runoff. This is consistent with the comparison in Figure 6 which indicates slightly lower observed salinity in the Strait of Georgia. For the experiment with increased river discharge, the summer maximum is close to the levels of 1999, the year with the largest river discharge for the period considered. These results point to a possible underestimation of freshwater discharge used to force the basic experiment. They also indicate that the range in freshwater content of the model varies within the observed range under typical inter-annual changes in the freshwater forcing.

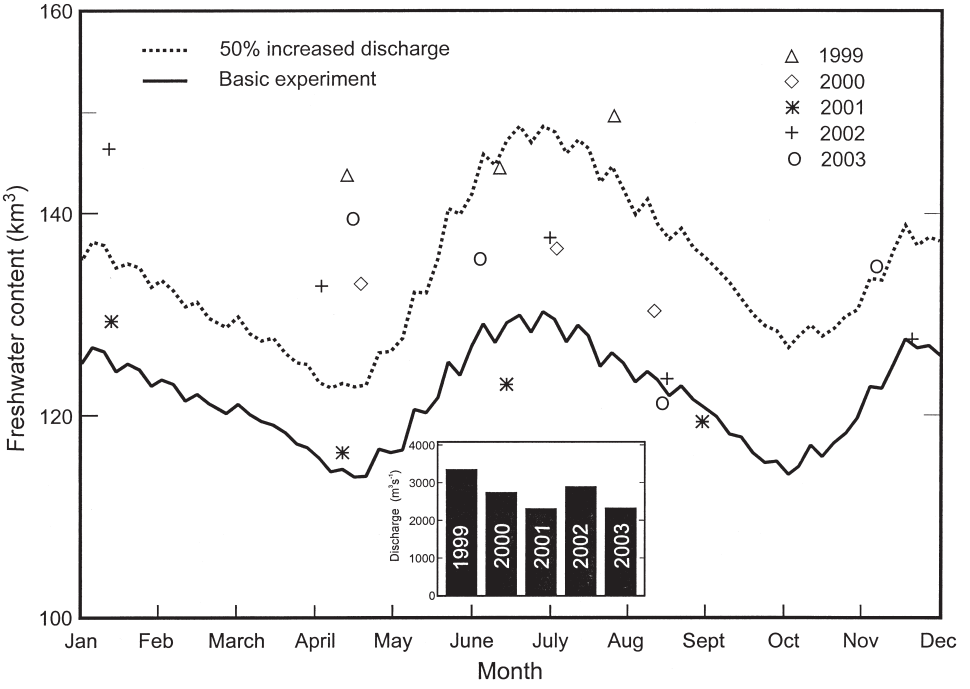

Figure 13. Total freshwater content of the coastal basin for the basic experiment (full line) and for the case with 50% increase in freshwater inflow (dotted line). Also included are estimates from the 19 hydrographic surveys carried out from 1999 to 2003. The small bar plot gives the mean annual Fraser river discharge for the years 1999 to 2003.

Aside from the dominant influence of buoyancy forcing, the dynamics of the estuary are also thought to be controlled by vigorous tidally-induced mixing, particularly in the vicinity of the shallow sills of the southern Strait of Georgia. This locally intensified vertical mixing results in reduced stratification in Haro Strait and is important in maintaining the along-strait salinity gradient (e.g. Fig. 6). The effect of the tide on vertical mixing can be assessed by comparing results from numerical integrations with and without tidal forcing. To do so, a 50 day integration period starting with conditions prevailing on Nov. 16 in the third year of the reference experiment was repeated, but with tidal forcing turned off. An average of the vertical diffusivity coefficient over this 50 day period was then computed for this case and is compared to a similar average for the reference experiment in Figure 14. It is evident that vigorous tidal currents in Haro Strait are associated with a strong localized maximum in the vertical mixing coefficient. This feature is consistent with the results of Foreman *et al.* (1995) who estimated that 36% of the tidal energy flux from eastern Juan de Fuca is dissipated before entering the Strait of Georgia.

The small-scale processes which produce the vigorous mixing in Haro Strait (e.g. Farmer *et al.,* 2002) are obviously not simulated in the model. However, given the model's

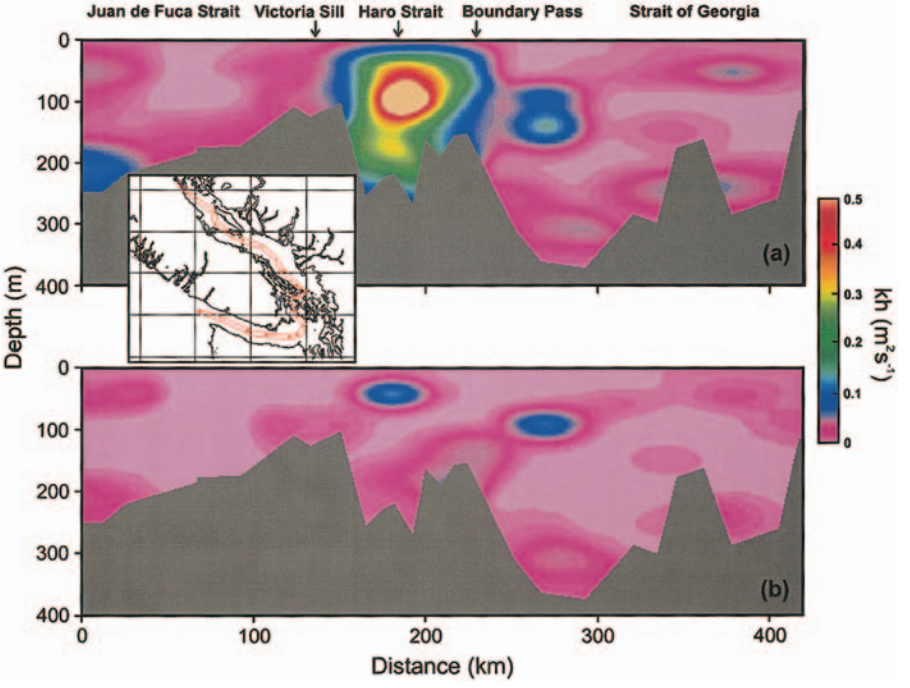

Figure 14. Vertical diffusivity mixing coefficient averaged over a 50-day winter period starting in November of the third year of the reference experiment (a), and for the case in which tidal forcing is omitted during this 50-day period (b).

ability to reproduce the measured salinity structure (see Fig. 6), the overall level and distribution of mixing given by the turbulence closure scheme appears to be adequate. The reason may be that the tidally induced turbulent mixing in Haro Strait is, at times, large enough to completely homogenize the water column. Additional turbulence can not then lead to further buoyancy fluxes. As long as the model produces this "saturation" level of mixing, the precise magnitude and distribution of the vertical mixing coefficients may not be important. The comparison of Figure 14 reveals that the tidal forcing is a significant contributor in setting up the locally enhanced mixing in Haro Strait, causing a many-fold increase in the local vertical mixing coefficient. Consequently, the vigorous tidal currents have an important influence on the control of the estuarine exchange flow. Salinity contours obtained at the end of the 50-day period along the estuary's thalweg are given in Figure 15. It is clear that, in the case without tidal forcing (Fig. 15b), the stratification within Haro Strait is now too strong and the overall lateral salinity (density) gradient within the estuary is too small.

The role of wind forcing in determining the response of the system at seasonal time scale was also considered. The reference experiment was repeated but with the wind stress forcing omitted. The resulting salinity structure and its seasonal cycle (not shown) are

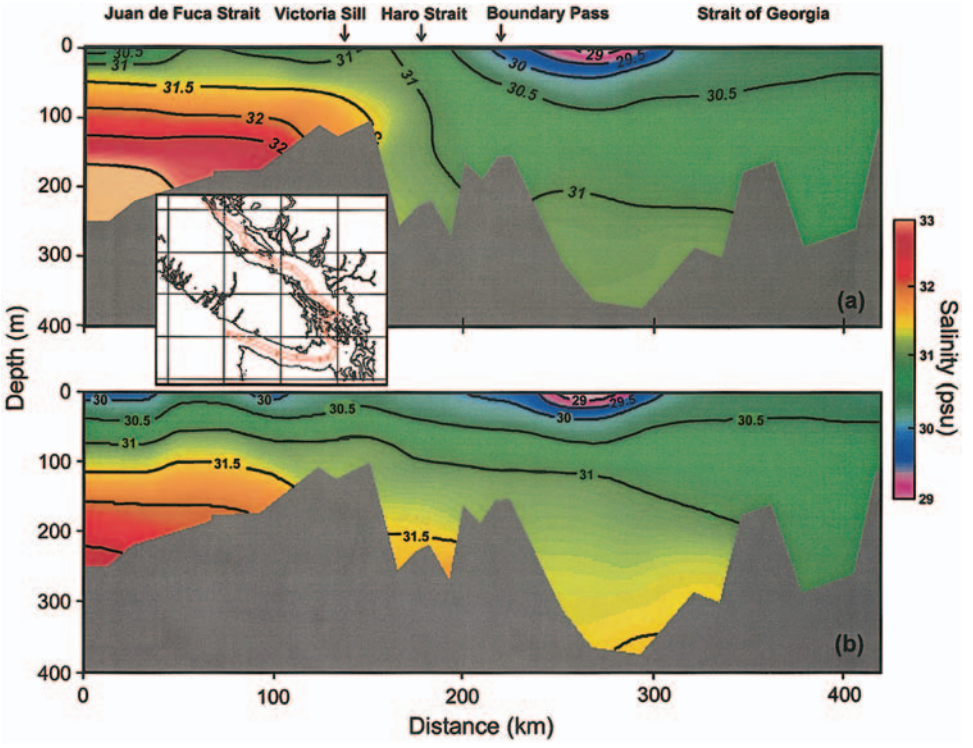

Figure 15. Along-strait section of salinity averaged over the last 5 days of the 50-day period of Figure 14, for the basic experiment (a), and for the case without tidal forcing (b).

similar to that of the reference case. There is a small decrease in the salinity of the surface river plume near the mouth of the river due to reduced near-surface mixing, but no significant change in its position. Accordingly, the seasonal cycle of wind stress does not appear to be a determining factor in establishing the main features of the seasonal cycle of the water properties within the estuary.

Lateral mixing which is included here for reasons of numerical stability and is dependent on model resolution, can produce spurious diapycnal mixing. In the POM, the "horizontal mixing" is along the sloping sigma levels and may lead to diapycnal mixing where density surfaces intersect sigma levels (Mellor and Blumberg, 1985). An additional experiment was performed to examine the sensitivity of the model results to the choice of the coefficient (HORCON) governing the Smagorinsky diffusivity parameterization (Smagorinsky, 1963). In the reference experiment HORCON was set to a relatively small value of 0.03. The reference case was repeated but with the value of HORCON doubled to 0.06. The change in HORCON mostly affects subsurface salinity values within the Strait of Georgia (Fig. 12c). The larger HORCON value leads to increased mixing of the deep estuarine return flow entering the Strait of Georgia with the upper fresher layer. This occurs over the

Southern strait where large salinity gradients are present over the sill area. This extra dilution of the salty, sub-surface intrusions leads to an unrealistic freshening of the deep Strait of Georgia. Overall, increasing HORCON has deleterious effects on the quality of the simulations. The general recommendation to keep horizontal diffusion as small as possible (e.g. Becker *et al.,* 2002) is apparently valid here.

4. Conclusions

The Strait of Georgia/Juan de Fuca estuary is a complex system with significant variability on a wide range of time scales. The present study combined new observations from a recent series of hydrographic cruises with historical observations to provide a comprehensive view of the circulation and seasonal variations in the mass field. A particular focus of this study has been on a comparison of the mean stratification and the seasonal variability with a fully prognostic numerical model of the region driven by climatological forcing.

The comparison between the simulations and observations indicates that the most prominent aspects of the mean salinity (and density) field along the main axis of the estuary are well represented by the model. This includes the shallow front over Boundary Pass, the deep front over Victoria Sill and the well mixed waters of Haro Strait. The inclusion of tidally-induced mixing is showed to be important in this regard. The results also indicate that the mean circulation gyre observed in the Strait of Georgia is a component of the estuarine-driven flow and that the volume exchange is significantly larger in the southern access to the estuary. In addition, model results indicate that wind forcing plays a relatively minor role in establishing the mean climatology and seasonal variability of the Strait of Georgia.

Perhaps the most important discrepancy with the observed time-averaged salinity is that the surface freshwater plume within the Strait of Georgia is too confined to the south and does not extend over the northern strait as much as observed (e.g. Fig. 6). This suggests that runoff into the northern strait may not be represented adequately. At present, there is insufficient information on the freshwater runoff from numerous small streams into the northern strait and adjoining inlets. The discrepancy may also point to the need to improve salinity values specified at the northern open boundary of the model. These conditions are important in controlling the estuarine exchange at the northern end of the strait. The observational database over this area is relatively sparse and should be improved.

Seasonal variations of salinity are reasonably well represented for Juan de Fuca Strait. The model captures the biannual salinity minima near the surface and the summer salinity maximum observed at depth. The latter is controlled by the upwelling produced by offshore winds. On the other hand, representation of seasonal variability in the deep Strait of Georgia is a more difficult problem.

Deep water renewal involves the mixing and advection of surface and deep water masses such that water masses are produced that are dense enough to penetrate the deep basin twice a year, during the spring and fall seasons. On the other hand, in the model, the most

intense deep water renewal happens in early summer. One reason may be that temperature variability has not been included in the numerical simulations. Consequently, the model did not allow for the summer warming and winter cooling of the surface waters that may influence the seasonal changes of mixture involved in the formation of the deep water intrusions. This matter will be addressed in future work.

The continuation of the monitoring program and of the associated hydrographic time series will permit us to address the problem of variability at inter-annual time scales and, ultimately, the problem of regional climate change. For example, the surveys have shown that inter-annual variations in freshwater content occur as a response to inter-annual changes in river discharge (Fig. 13). The numerical model developed for the present study will be a valuable tool in such an investigation.

Acknowledgments. We thank Emilie Davenne for her data analysis and general insight into the problem and Lizette Beauchemin for preparing the figures. Some figures were prepared with the help of the ODV software (Schlitzer, 2002). We also thank Mitsuhiro Kawase for useful discussions.

REFERENCES

Beckers, J.-M., M. Rixen, P. Brasseur, J.-M. Brankart, A. Elmoussaoui, M. Crépon, Ch. Herbaut, F. Martel, F. Van den Berghe, L. Mortier, A. Lascaratos, P. Drakopoulos, G. Korres, K. Nittis, N. Pinardi, E. Masetti, S. Castellari, P. Carini, J. Tintore, A. Alvarez, S. Monserrat, D. Parrilla, R. Vautard, and S. Speich. 2002. Model intercomparison in the Mediterranean: MEDMEX simulations of the seasonal cycle. J. Mar. Syst., *33–34,* 215–251.

Blumberg, A. F. and G. L. Mellor. 1987. A description of a three-dimensional coastal ocean circulation model, *in* Three Dimensional Coastal Ocean Models, N. Heaps, ed., Coastal Estuarine Sci. Ser., *4,* Amer. Geophys. Union, 1–16.

Crean, P. B., T. S. Murty and J. A. Stronach. 1988. Mathematical Modelling of Tides and Estuarine Circulation, Springer-Verlag, NY, 471 pp.

England, L. A., R. E. Thomson and M. G. G. Foreman. 1996. Estimates of seasonal flushing times for the southern Georgia Basin, Can. Tech. Rep. Hydrogr. Ocean Sci., *173,* 24 pp.

Farmer, D., R. Pawlowicz and R. Jiang. 2002. Tilting separation flows: a mechanism for intense vertical mixing in the coastal ocean. Dyn. Atmos. Oceans, *36,* 43–58.

Flather, R. A. 1987. A tidal model of the northeast Pacific. Atmos.-Ocean, *25,* 22–45.

Foreman, M. G. G., R. A. Walters, R. F. Henry, C. P. Keller and A. G. Dolling. 1995. A tidal model for eastern Juan de Fuca Strait and the southern Strait of Georgia. J. Geophys. Res., *100(C1),* 721–740.

Freeland, H. J., W. R. Crawford and R. E. Thomson. 1984. Currents along the Pacific coast of Canada. Atmos.-Ocean, *22,* 151–172.

Griffin, D. A. and P. H. LeBlond. 1990. Estuary/ocean exchange controlled by spring-neap tidal mixing. Estuar. Coast. Shelf Sci., *30,* 275–297.

Herlinveaux, R. H. and J. P. Tully. 1961. Some oceanographic features of Juan de Fuca Strait. J. Res. Bd. Canada, *18(6),* 1027–1071.

Holloway, G. 1993. On residual currents in the central Strait of Georgia, B.C. Atmos.-Ocean, *31,* 167–170.

LeBlond, P. H. 1983. The Strait of Georgia: functional anatomy of a coastal sea. Can. J. Fish. Aquat. Sci., *40,* 1033–1063.

LeBlond, P. H., K. Dyck, K. Perry and D. Cumming. 1983. Runoff and precipitation time series for

the coasts of British Columbia and Washington State. Dept. of Oceanography, University of British Columbia Rep. 39, 133 pp.

LeBlond, P. H., D. A. Griffin and R. E. Thomson. 1994. Surface salinity variations in the Juan de Fuca Strait: test of a predictive model. Cont. Shelf Res., *14,* 37–56.

Li, M., A. Gargett and K. Denman. 1999. Seasonal and interannual variability of estuarine circulation in a box model of the Strait of Georgia and Juan de Fuca Strait. Atmos.-Ocean, *37,* 1–19.

Marinone, S. G. and J. Fyfe. 1992. Residual currents in the central Strait of Georgia, B.C. Atmos.-Ocean, *30,* 94–119.

Marinone, S. G., S. Pond and J. Fyfe. 1996. A three-dimensional model of tide and wind-induced residual currents. Estuar. Coast. Shelf Sci., *43,* 157–182.

Masson, D. 2002. Deep water renewal in the Strait of Georgia. Estuar. Coast. Shelf Sci., *54,* 115–126.

Masson, D. and P. F. Cummins, 1999. Numerical simulations of a buoyancy-driven coastal countercurrent off Vancouver Island. J. Phys. Oceanogr., *29,* 418–435.

—— 2000. Fortnightly modulation of the estuarine circulation in Juan de Fuca Strait. J. Mar. Res., *58,* 439–463.

Mellor, G. L. and A. F. Blumberg. 1985. Modeling vertical and horizontal diffusivities with the sigma coordinate system. Mon. Weath. Rev., *113,* 1380–1383.

Mellor, G. L. and T. Yamada. 1982. Development of a turbulent closure model for geophysical fluid problems. Rev. Geophys. Space Phys., *20,* 851–875.

Schlitzer, R. 2002. Ocean Data View, *http://www.awi-bremerhaven.de/GEO/ODV.*

Smagorinsky, J. 1963. General circulation experiments with the primitive equations: 1. the basic experiment. Month. Weath. Rev., *91,* 99–164.

Stacey, M. W., S. Pond, P. H. LeBlond, H. J. Freeland and D. M. Farmer. 1987. An analysis of the low-frequency current fluctuations in the Strait of Georgia, from June 1984 until January 1985. J. Phys. Oceanogr., *17,* 326–342.

Thomson, R. E. 1976. Tidal currents and estuarine-type circulation in Johnstone Strait, British Columbia. J. Fish. Res. Board Can., *34(5),* 697–703.

—— 1981. Oceanography of the British Columbia Coast. Can Spec. Publ. Fish. Aquat. Sci., *56,* 291 pp.

Waldichuk, M. 1957. Physical Oceanography of the Strait of Georgia, British Columbia. J. Fish. Res. Bd. Canada, *14(3),* 321–486.

Webster, I. 1977. A physical oceanographic study of Haro Strait: a data summary and preliminary analysis. Contract. Rep. Ser., 77-3, Inst. Of Ocean Sci., Sidney, B.C.

Young, E. F., J. Brown, J. N. Aldridge, K. J., Horsburgh and L. Fernand. 2003. Development and application of a three-dimensional baroclinic model to the study of the seasonal circulation in the Celtic Sea. Cont. Shelf Res., *24,* 13–36.

Zavatarelli, M., N. Pinardi, V. H. Kourafalou and A. Maggiore. 2002. Diagnostic and prognostic model studies of the Adriatic Sea general circulation: Seasonal variability. J. Geophys. Res., *107(C1),* 4.1–4.20.

Received: *30 June, 2003;* revised: *11 May, 2004.*